Korean J. Chem. Eng., 34(1), 41-53 (2017)
DOI: 10.1007/s11814-016-0221-4

pISSN: 0256-1115
eISSN: 1975-7220

Structural evolution of hierarchical porous NiO/Al_2O_3 composites and their application for removal of dyes by adsorption

Jian Rong*, Tao Zhang*,, Fengxian Qiu*,†, and Mingliang Chen***

*School of Chemistry and Chemical Engineering, Jiangsu University, Zhenjiang 212013, Jiangsu Province, China
**Institute of Green Chemistry and Chemical Technology, Jiangsu University, Zhenjiang 212013, Jiangsu Province, China
(*Received 23 April 2016 • accepted 1 August 2016*)

Abstract−Hierarchical porous NiO/Al_2O_3 composites were successfully prepared by two-steps. First, the core-shell structured Al_2O_3 microspheres were prepared via a template-free hydrothermal route using $KAl(SO_4)_2 \cdot 12H_2O$ and $Al_2(SO_4)_3 \cdot 18H_2O$ as aluminum source. Then, the NiO/Al_2O_3 composites with micro- and nano-hierarchical structures were prepared by a hydrothermal method combining the subsequent calcination process. The obtained characterization result presented that the morphology of hierarchical Al_2O_3 microsphere tuned to irregular platelets by simply varying Ni/Al ratios. The BET analysis showed that the special surface area from 52.12 $m^2\ g^{-1}$ to 214.8 $m^2\ g^{-1}$ after two hydrothermal complex process. Effects of Ni/Al ratio, adsorbent dosage, Congo red (CR) concentration, coexisting ions, adsorption time and temperature were investigated. The obtained results indicated that NiO/Al_2O_3 composite had the high adsorption efficiency (99.6%) and great adsorption capacity (186.9 mg g^{-1}) under the optimum conditions. The adsorption isotherm and kinetics data were found to be well fitted and in good agreement with the Langmuir isotherm model and pseudo-second order model, respectively. The hierarchical porous NiO/Al_2O_3 composites presented remarkably higher adsorption efficiency during five recycling, which showed their potential as the highly efficient adsorbent for removal of CR in wastewater.

Keywords: NiO/Al_2O_3, Hierarchical Porous Material, Congo Red, Adsorption

INTRODUCTION

With an awareness toward the improvement of health and environment, great concern has arisen on water pollution, especially for dyes, which are widely used in various fields, such as textile [1], paper [2], rubber plastics [3], printing [4] and so forth. Among diverse dyes, Congo red (CR) is one of anionic azo dyes with the azo bond (-N=N-), which are toxic [5], carcinogenic [6] and even recalcitrant due to their inertia [7]. Every year, more than 100 tons of various types of dye are discharged into rivers and lakes [8]. Taking into account the safety of biota and animal groups, it is necessary to remove the dye pollutants from water. Recently, various technologies have been used for removal of noxious dyes such as oxidation [9], precipitation [10], adsorption [11] and flocculation [12]. However, several disadvantages also exist in the most of these methods listed above, such as low efficiency, low recovery rate, secondary pollution and so on. Considered overall, adsorption technology has attracted keen attention in disposing wastewater due to its excellent cycle performance, simple operation and low cost. Therefore, it is very important to design new adsorbents with high adsorption capacities and good reusability and to develop new synthetic procedures for preparing such porous materials.

Among various alternative materials, aluminum oxides (Al_2O_3) have been widely used in various fields such as adsorption, catalysis, electrochemistry and sensors due to high specific surface area, high porosity and excellent physical-chemical properties, moreover aluminum oxides itself are low toxicity and cost [13]. In particular, nanostructured Al_2O_3 has garnered a considerable amount of attention for its excellent surface properties. Many nanostructured Al_2O_3 materials have been investigated such as nanorods [14], nanowires [15], nanofibers [16], nanoplates [14], core/shell nanocomposites [17], and 3-D mesoporous [18] structures for applications in adsorption and catalysis. Nevertheless, two key fundamental issues remain to be addressed to fully utilize the advantages of the structural characteristics. One problem is that the high surface energy of nano-Al_2O_3 makes them extremely reactive, and most systems undergo aggregation without protection of their surfaces [14]. The other problem is the lack of active sites for the adsorption of anionic dyes. Combined with previous studies, hence, control of structure and modification of functional material could be significantly improved in terms of adsorption [13,19,20].

On the one hand, hierarchical structure materials have been attracting extensive research interest, because its structures combine the features of micrometer-and nanometer-scaled building blocks and have unique properties distinct from those of the monomorphological structures [21]. For applications in adsorption and catalysis, both micrometer-and nanometer-scaled morphologies are required to be presented in the materials to achieve highly organized functions. The micrometer-sized overall structure provides the necessary mechanical robustness against wear and tear, while their nanostructure provides a high surface area. Thus, the controlled fabrication of hierarchically structured Al_2O_3 adsorbent with

†To whom correspondence should be addressed.
E-mail: fxqiu@126.com

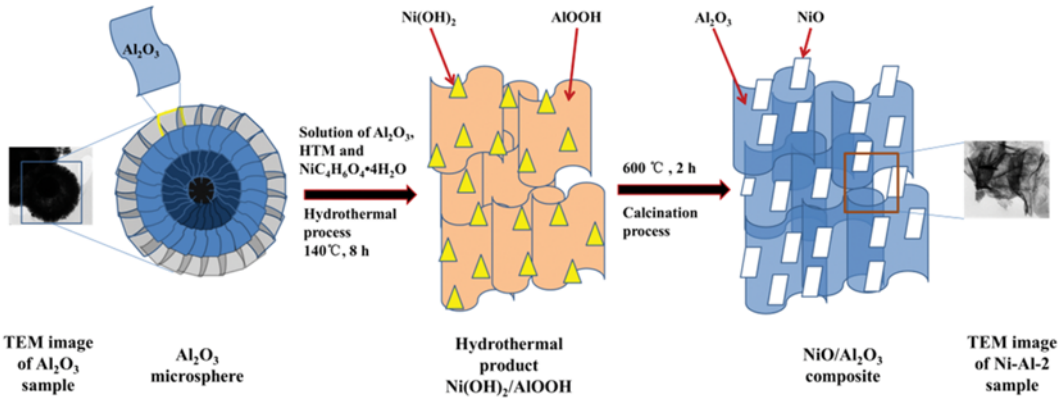

Scheme 1. The synthetic route of NiO/Al_2O_3 adsorbent.

tunable composition, structure and functionality is important from the fundamental and application point of view.

On the other hand, nickel oxide (NiO) is a significant functional adsorption material due to the strong attraction force between adsorbate and the surfaces of material. As an adsorbent, NiO, a positive charge material with high theoretical capacity [22], will be a potential and efficient adsorbent for anionic dyes. Nevertheless, the potential application of NiO for dye adsorption was limited due to its very low specific surface area and low adsorption capacity [23]. Then, to the best of our knowledge, there is no report about NiO/Al_2O_3 composites by the synthetic method of a hydrothermal method combining a subsequent calcination process.

We prepared highly porous NiO/Al_2O_3 composites by a two-step method, which is simple, efficient, and highly reproducible. Enhanced CR adsorption properties could be possibly achieved by the combination of the hierarchical structures of composites with the functionality of NiO and Al_2O_3. To study the potential and effectiveness of the hierarchical porous NiO/Al_2O_3 composites for the adsorption of the CR dyes from the wastewater, we considered various parameters affecting the adsorption efficiency, such as amount of adsorbent, concentration, temperature, contact time, interfering ions and recycling on removal efficiency, which were well studied and optimized. The adsorption isotherm and kinetics for CR adsorption onto NiO/Al_2O_3 composites were also studied. In addition, a tentative mechanism of CR adsorption on NiO/Al_2O_3 composites was discussed in detail.

MATERIALS AND METHODS

1. Materials

Aluminum potassium sulfate dodecahydrate ($KAl(SO_4)_2{\cdot}12H_2O$), aluminium sulfate octadecahydrate $Al_2(SO_4)_3{\cdot}18H_2O$, urea ($CO(NH_2)_2$), nickel acetate tetrahydrate ($NiC_4H_6O_4{\cdot}4H_2O$) and hexamethylenetetramine ($C_6H_{12}N_4$, HTM) were of analytical grade. They were used without further purification. All water used was distilled. CR (formula: $C_{32}H_{22}N_6Na_2O_6S_2$, molecular weight: 696.67 g mol^{-1}, λ_{max}: 497 nm, molecular diameter: ~36 angstrom) used in the experiments was obtained from Aladdin Chemical Reagent Co. Ltd., and the molecular structure of CR was provided in supplementary information (see Fig. S1).

2. Preparation of Hollow Al_2O_3 Microspheres

In a typical experiment, 3 mmol of $KAl(SO_4)_2{\cdot}12H_2O$, 1 mmol $Al_2(SO_4)_3{\cdot}18H_2O$ and 8 mmol of $CO(NH_2)_2$ were added to 80 mL of distilled water. Then, the mixture was transferred to a 100 mL Teflon-lined autoclave, sealed and heated 180 °C for 3 h. After cooling to room temperature naturally, the products were collected by centrifugation, washed with distilled water and ethanol for several times, the washed samples were dried at 80 °C for 12 h. Finally, the sample was calcined at 600 °C with ramping rate of 3 °C min^{-1} and then kept for 2 h to obtain the hollow Al_2O_3 microspheres.

3. Preparation of NiO/Al_2O_3 Composites

The NiO/Al_2O_3 coupled adsorbents were synthesized by a hydrothermal method combining a subsequent calcination process, as described in Scheme 1. 2 mmol of Al_2O_3, 1 mmol of $NiC_4H_6O_4{\cdot}4H_2O$ and 4 mmol of HTM were first dissolved in 60 mL of distilled water, the solution was hydrothermally 140 °C for 8 h. In this reaction, HTM acted as precipitating agent and a source of OH^- that combined with Ni^{2+} and Al^{3+}. Then the product was collected by centrifugation, washed with the distilled water ethanol for several times, dried in 80 °C for 12 h to obtain $Ni(OH)_2$/AlOOH composite. The final product was calcined at 600 °C for 2 h to form the NiO/Al_2O_3 composites. To simplify, the composite was denoted as Ni-Al-1 ($n_{Ni}:n_{Al}=1:4$). Then, a series of NiO/Al_2O_3 composites with different proportions ($n_{Ni}:n_{Al}=1:3$, 1 : 2 and 1 : 1) were prepared and re-marked as Ni-Al-2, Ni-Al-3, Ni-Al-4, respectively. As a comparison, NiO/Al_2O_3 and CR was prepared by a simple mechanical mixing, denoted as NiO/Al_2O_3-CR.

4. Characterization

The products were characterized by X-ray diffraction (XRD) analysis (type HZG41 B-PC). Radial scans were recorded in the reflection scanning mode from 2θ=5-80° with a scanning rate of 4° min^{-1}. The size and morphology of the nano-structure were scanned on a PHI-Tecnai 12 transmission electron microscope (TEM), scanning electron microscopy (SEM) and energy-dispersive X-ray spectroscopy (EDS). The Brunauer-Emmett-Teller (BET) surface area of each powder was measured by nitrogen adsorption in a Micromeritics ASAP 2020 nitrogen adsorption apparatus (USA). The specific surface area and the total specific volume of the pores were calculated by the BET method and BJH method, respectively. FTIR analysis was carried out in the range of 400-4,000 cm^{-1} using a

FTIR spectrophotometer (Thermo Nicolet, NEXUS, TM) in KBr pellets.

5. Batch Adsorption Experiment for Congo Red

The CR aqueous solution could serve as wastewater. The adsorption performance of NiO/Al_2O_3 was evaluated by investigating the adsorption removal of CR from aqueous solutions. The effects of dye concentration (50-500 mg L^{-1}), temperature (293 K, 313 K and 333 K), amount of adsorbent (10-100 mg), contact time (0-90 min), interfering ions (Cl^-, CO_3^{2-} and SO_4^{2-}) and recycling on removal efficiency were studied to assess potential applications for treating wastewater.

Batch adsorption experiments were carried out in this work. After each adsorption experiment, the dye solution was centrifuged (10,000 rpm, 5 min) using a centrifuge for separating the adsorbent from aqueous solutions. The supernatant was analyzed by UV-vis spectrophotometry (UV-2550) at the characteristic absorption peak of 497 nm. The concentration of the CR could be calculated according to the work curve previously drawn. The CR removal efficiency, D, was calculated as follows:

$$D = \frac{C_o - C_t}{C_o} \times 100\%$$

where C_o and C_t are the initial concentration and the concentration at time t (mg L^{-1}), respectively. The amount of CR adsorbed per unit adsorbent (q_e, mg g^{-1}) was calculated according to a mass balance on the CR concentration using the equation:

$$q_e = \frac{V(C_o - C_e)}{m}$$

where V (L) is the volume of CR solution, m (g) is the mass of the NiO/Al_2O_3 adsorbent (g), and C_e (mg L^{-1}) is the equilibrium concentrations of CR. The adsorption amount was calculated according to the following Equation:

$$q_t = \frac{V(C_o - C_t)}{m}$$

where the q_t (mg g^{-1}) is the amount of adsorbed by the NiO/Al_2O_3 composites, C_t (mg L^{-1}) is the concentrations of CR at time t.

6. Cycle Experiment

The reusability study was carried out immediately after the adsorption equilibrium. The saturated NiO/Al_2O_3 composites were collected and separated by centrifugation, washed with distilled water and ethanol for several times to remove the surface excess CR dye, followed by drying at 80 °C for 12 h. Next, the sample was calcined at 500 °C for 2 h to get rid of the dye on the adsorbent. Finally, 30 mg of the recovered sample was put into 20 mL of CR solution (200 mg L^{-1}), and the mixture was then placed in a water bath to reach adsorption equilibrium. Such an experiment was repeated five times.

RESULTS AND DISCUSSION

1. Results of Al_2O_3 Microspheres

The morphology and microstructure of the as-prepared Al_2O_3 sample were shown by SEM and TEM images. As can be seen from Fig. 1(a), the Al_2O_3 powders were evenly distributed microspheres with a diameter of 4.0-5.0 μm. As shown in Fig. 1(b) the

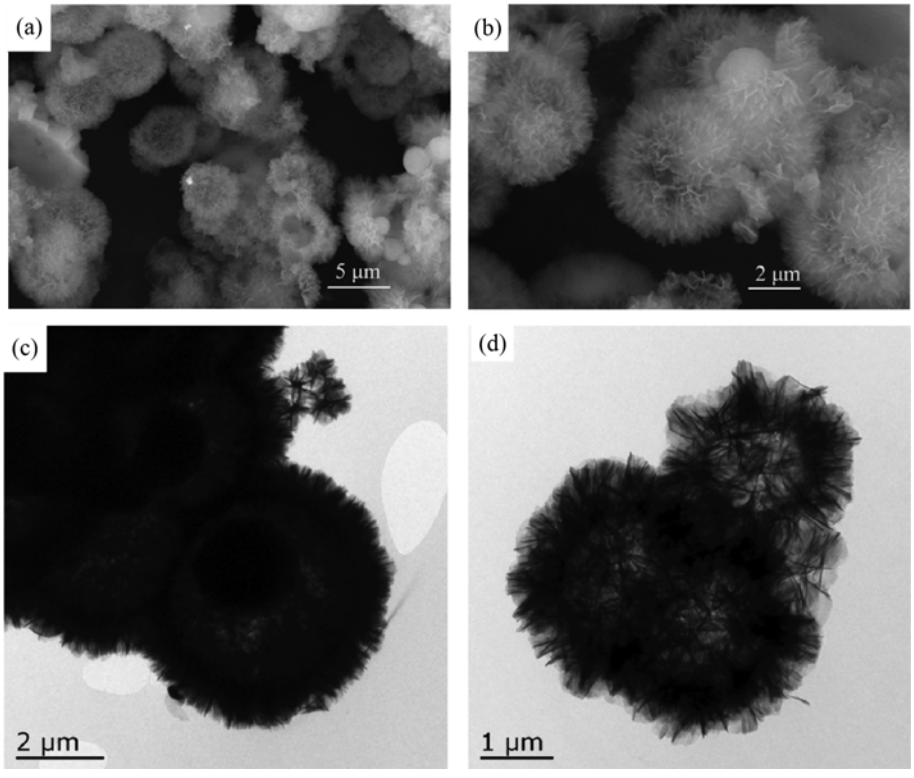

Fig. 1. SEM (a) and (b) and TEM (c) and (d) images of the hollow Al_2O_3 samples at different magnifications.

surfaces of Al_2O_3 microspheres were formed by self-assembly of nanosheets. These nanosheets can provide high specific surface areas and porous structures. TEM image of the pure Al_2O_3 (Fig. 1(c) and (d)) further demonstrated that these microspheres were hollow, with a flower-like hierarchical structure of nanosheets, and the diameter of each hollow microsphere was approximately 5.0 μm. The corresponding TEM image depicted in Fig. 1(c) also demonstrated a core is self-enclosed in the hollow shell to construct core-shell structure.

Fig. 2(a) represents the XRD patterns of the as-prepared Al_2O_3 microspheres obtained at the calcination temperature of 600 °C. All the diffraction peaks are indexed to γ-Al_2O_3 (JCPDF card, No. 10-0425) [18]. The XRD pattern of prepared samples exhibit broad peaks with weak intensities most probably due to the poorly crystalline γ-Al_2O_3. Similar results were observed in the literature of other γ-Al_2O_3 materials prepared by template method [15]. No obvious XRD peaks arising from other crystalline forms of alumina were observed, indicating the high purity of the as-prepared Al_2O_3 samples [24,25]. The special surface area of the hollow Al_2O_3 was determined by nitrogen adsorption measurements (Fig. 2(b)). The calculated specific surface area, total pore volume and pore size were 52.12 m^2 g^{-1}, 0.13 cm^3 g^{-1} and 25.43 nm, respectively. The pore size distribution of the sample is described in the insert picture of Fig. 2(b). The dominant pore size ranged from 20 to 30 nm, which confirmed the Al_2O_3 samples have a structure of mesopore and contain a very high pore volume.

2. Results of NiO/Al_2O_3 Composites

The Ni/Al molar ratios influence the composition, structure and

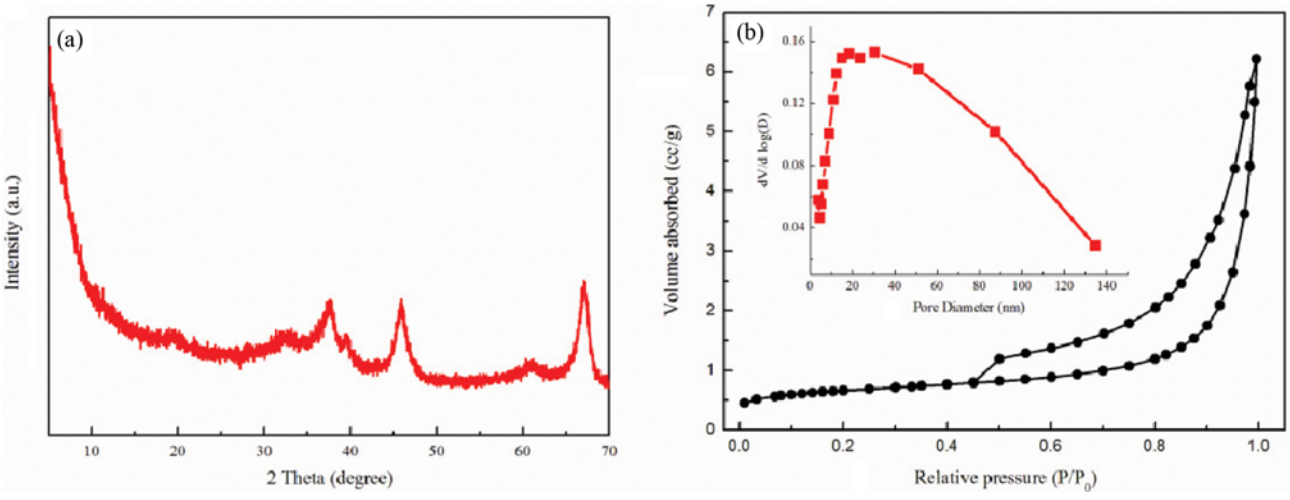

Fig. 2. XRD pattern (a) of the Al_2O_3 sample; nitrogen adsorption-desorption isotherms and corresponding pore-size distribution curves (inset) for Al_2O_3 (b).

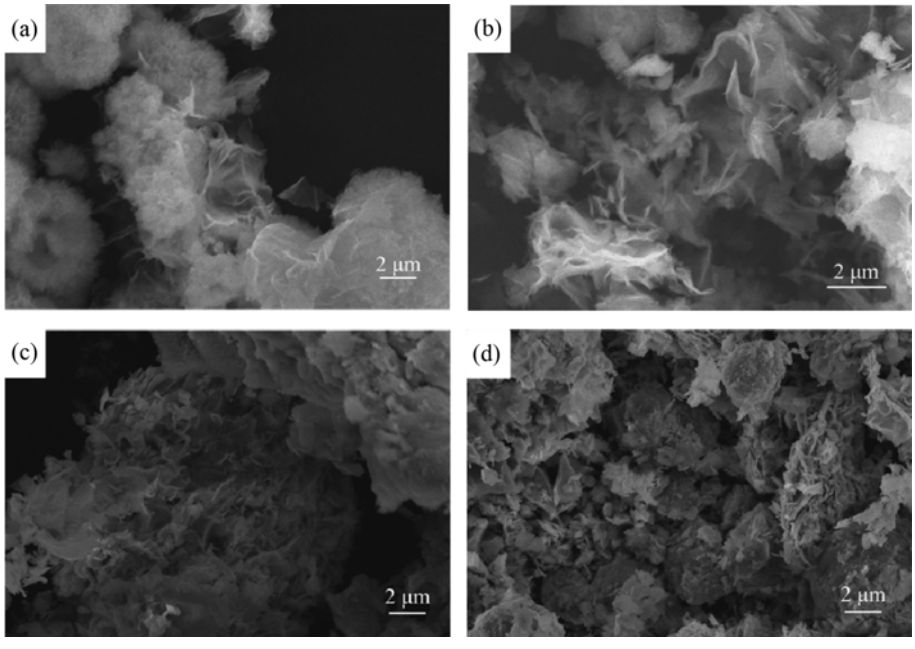

Fig. 3. SEM images of the Ni-Al-1 (a), Ni-Al-2 (b), Ni-Al-3 (c) and Ni-Al-4 (d).

morphology of composites by controlling the extent of Al_2O_3 surface reaction, thus affecting the CR adsorption. To directly observe the microstructures and morphologies evolution of NiO/Al_2O_3 composites, Ni/Al molar ratios-dependent evolutions of structural morphology was investigated by SEM, EDS, TEM, XRD and BET surface area analysis. Fig. 3 illustrates the morphology evolution at various Ni/Al molar ratios. It indicated that the microstructures of hierarchical NiO/Al_2O_3 composites could be tuned from microsphere morphology to irregular platelets by controlling the Ni/Al molar ratios. It can be seen from Fig. 3(a) that spherical morphologies were still retained in NiO/Al_2O_3 composites, with a small amount of nanosheets. However, the structure of composites changed greatly with further increasing the Ni/Al molar ratios. As shown in Fig. 3(b), the SEM image of NiO/Al_2O_3 composites showed an irregular 2-D plate-like morphology with the majority crystallites ranging from 2 to 5 μm in size. The thin plate-like structures could provide the high surface area for CR adsorption. Fig. 3(c) and (d) displays the SEM images of Ni-Al-3 and Ni-Al-4 composites. In morphology, the nanoplates were aggregated into bulky particles with irregular shapes. In addition, in Fig. 3(c) and (d) the thickness of the NiO/Al_2O_3 composites plates was larger than that of the sheets in Fig. 2(b). The agglomerated structures of composites are not favorable for CR adsorption. Furthermore, the elemental distribution of Ni-Al-2 sample was investigated using energy-dispersive X-ray spectroscopy (EDS) (shown in Fig. S2 and S3). The elements of Ni, Al and O are displayed in different colors. Note that three elements showed uniform distribution without existence of other elements, and the element ratio of Ni and Al was close to 1/3.

To further study the nanostructure, the TEM images of Ni-Al-2 composites are shown in Fig. 4. Fig. 4(a), (b), (c) and (d) demonstrates Ni-Al-2 composites at low and high magnifications. It can be seen that the Ni-Al-2 sample composites have a heterogeneous

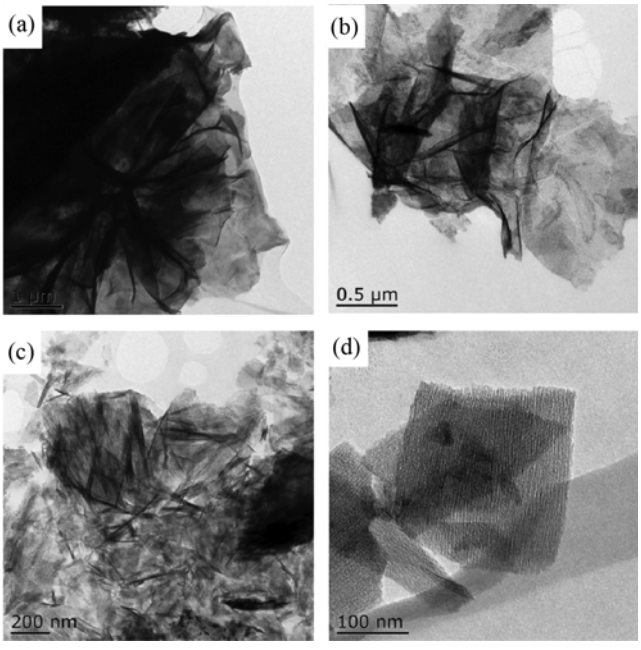

Fig. 4. TEM images of the Ni-Al-2 composite samples at different magnifications.

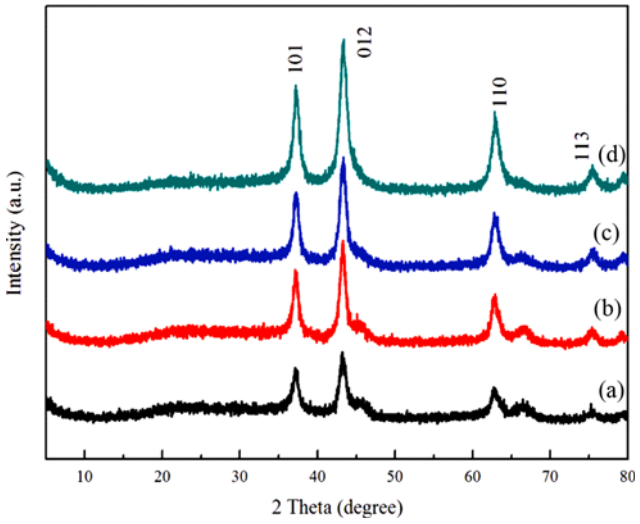

Fig. 5. XRD patterns of the Ni-Al-1 (a), Ni-Al-2 (b), Ni-Al-3 (c) and Ni-Al-4 (d) composites.

surface, which clearly demonstrates the formation of porous hierarchical architectures comprised of irregular nanoplatelets with homogeneous morphology. From Fig. 4(d), nanoplatelets were an ultrathin two-dimensional rectangular structure with a neat alternating-stripes surface, and the size of nanoplatelet was about several hundred nanometers from the lateral view. Compared with the TEM images of Al_2O_3, the core existing in the Al_2O_3 microspheres completely disappeared in the Ni-Al-2 composites by NiO synergistic effect undergoing the second hydrothermal process. This change could increase the special surface area of the sample to a large extent. Therefore, the dye molecules could be easily adsorbed on ultrathin surface layer via surface effects.

Fig. 5 shows the XRD patterns of NiO/Al_2O_3 composites prepared at different Ni/Al molar ratios. Compared with the pure Al_2O_3, the XRD patterns of NiO/Al_2O_3 composites only showed the characteristic peaks of NiO, which was attributed to the amorphous nature of Al_2O_3. As shown in Fig. 5, all of the relatively strong peaks, such as the peaks at 2θ=37.2, 43.2, 62.9 and 75.4°, could be assigned to the NiO crystal according to JCPDF card, No. 44-1159 [26], and the diffraction lines coincided with the (101), (012), (110) and (113) planes of the nickel oxide crystal. The reflection peaks of NiO became sharper, and their intensities were enhanced with increasing of the Ni/Al molar ratios, indicating the formation of ordered structures at higher Ni/Al molar ratios. It could be inferred from the SEM image (Fig. 3) that the enhanced crystallinity may be caused by a high degree of agglomeration of composite.

Fig. 6 shows a contrast nitrogen adsorption-desorption isotherms and pore-size distribution curves for Ni-Al-1, Ni-Al-2, Ni-Al-3 and Ni-Al-4. According to nitrogen adsorption-desorption isotherms for above four samples, the hysteresis in the pressure ranges p/p_0=0.4-1.0 indicated high level of textural porosities of the samples. The isotherm of all samples could be classified as IV-type with H3-type hysteresis loop caused by the capillary condensation of asymmetric slot-shape mesoporous and channels based on IUPAC classification of isotherms. A type H3 hysteresis loop indicated the asymmetric slot shape of mesoporous or channels in

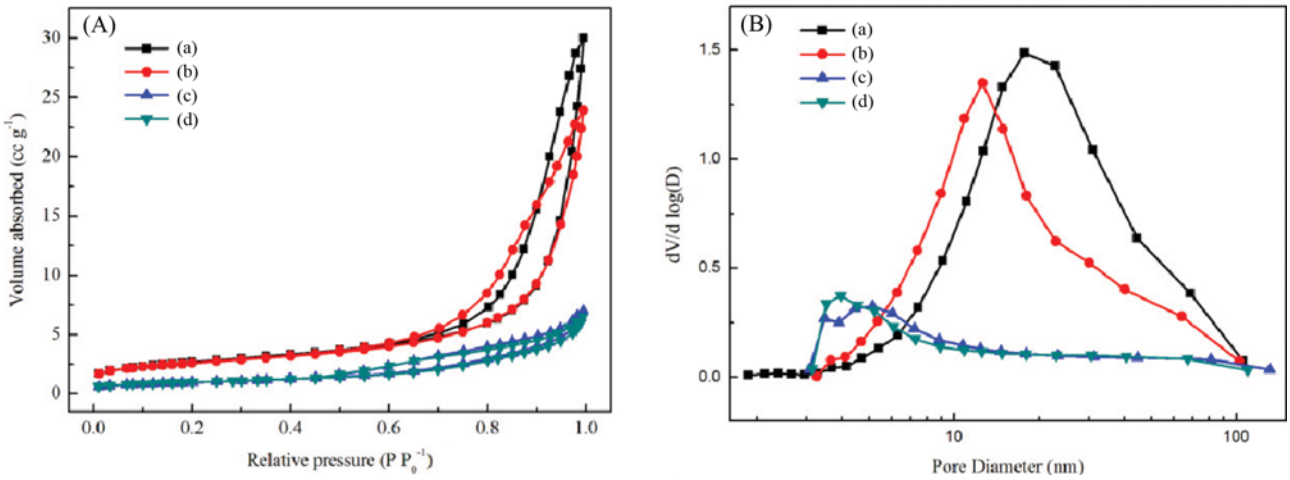

Fig. 6. Nitrogen adsorption-desorption isotherms (A) and corresponding pore-size distribution curves (B) for Ni-Al-1 (a), Ni-Al-2 (b), Ni-Al-3 (c) and Ni-Al-4 (d).

Table 1. Basic parameters for different Ni/Al molar ratios

Sample	S_{BET} (m^2 g^{-1})	V_{pore} (cm^3 g^{-1})	S_{pore} (nm)
Ni-Al-1	214.8	0.71	20.6
Ni-Al-2	205.7	0.64	17.9
Ni-Al-3	78.79	0.19	11.4
Ni-Al-4	77.41	0.17	11.3

agreement with the channel characteristics of irregular nanosheets.

Pore size distribution curves (Fig. 6(B)) were obtained from desorption branch of the isotherm by BJH method. The results indicated that the pore sizes decreased with increasing the Ni/Al molar ratio. Also, the pore size decreased from 20.7 nm to 17.9 nm as the Ni/Al molar ratio increased from 1/4 to 1/3. The pore structures may be formed by interconnected nanoplates. Thus, the decrease of pore size may be caused by aggregation of the nanoplates. More seriously, the pore size was dramatically decreased to about 11 nm as the Ni/Al molar ratio 1/2 and 1/1.

From Fig. 6, the special surface area and pore size decrease with the increase of the proportion of Ni. Hence, the NiO/Al_2O_3 composites prepared by in-situ growth successfully overcame the agglomeration of pure NiO nanoplates. Nevertheless, compared with pure Al_2O_3, the NiO/Al_2O_3 composites have higher special surface areas. This result could be explained from TEM result, which revealed the core existing in pure Al_2O_3 turned to nanoplates in composites. The BET surface area (S_{BET}), total pore volume (V_{pore}), and pore size (S_{pore}) of the four samples are listed in Table 1, further confirming that the composites Ni-Al-1 and Ni-Al-2 had higher specific surface area, total pore volume and pore size. Many researchers had proved mesopores and macropores were major positions for dye adsorption onto the composites materials [26,27]. Therefore, abundant porosity of adsorption materials could contribute to highly efficient dye adsorption.

3. Congo Red Adsorption

3-1. Effect of Ni/Al Molar Ratios

A comparative study for CR adsorption was carried out over the pure Al_2O_3 and the NiO/Al_2O_3 composites prepared at different Ni/Al molar ratios samples. Fig. 7 illustrates the effect of Ni/Al molar ratio on the adsorption efficiency of the CR onto the adsorbent. It can be found that the Ni-Al-2 composites had the highest adsorption efficiency (over 99.5%). Compared with pure Al_2O_3, the NiO/Al_2O_3 composites showed relatively high adsorption efficiency. The observed phenomenon could be possibly due to the increasing of special surface area and the loading of functional material NiO nanosheets. The result of BET presenting the special surface area of NiO/Al_2O_3 composites was 214.8 m^2 g^{-1}, which was much higher than that of the pure Al_2O_3 (52.12 m^2 g^{-1}). The high surface area provided more active sites, which resulted in higher adsorption efficiency. The low adsorption efficiency of Ni-Al-3 and Ni-Al-4 could be due to the low special surface area. On the other hand, according to Table 1, surface area and pore size of nickel-aluminum ratio of 1 : 3 were smaller than that of 1 : 4, implying that the functional material NiO also played an important role for CR adsorption. Similar phenomenon was also observed other Nickel-based materials for dye adsorption [28]. Considering

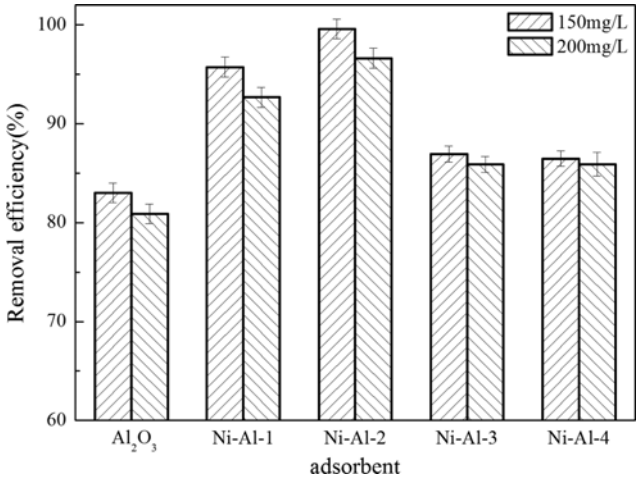

Fig. 7. Effect of Ni/Al molar ratios on CR adsorption (conditions: contact time, 120 min; adsorbent dose, 2 g L^{-1}; adsorption temperature, room temperature).

the adsorption efficiency, Ni-Al-2 (Ni/Al molar ratio=1/3) composites was fixed as optimum condition for the rest of the batch experiments.

3-2. Effect of Adsorbent Dosage

The effect of NiO/Al_2O_3 dosage on CR adsorption efficiency was studied, as shown in Fig. 8. It can be seen that removal efficiency of CR increased rapidly from 22.1% to 95.8% with the amount of adsorbent from 10 to 30 mg. This phenomenon could be caused by the increased rapidness of the active site for the CR interaction with the adsorbent. When dosage mass further increased from 50 to 100 mg, it had small effect of removal efficiency from 97.6% to 99.6%, which is in close proximity to 100% (complete removal). Nevertheless, the removal amount (q_e values) decreased with increase in adsorbent dosage. As shown in Fig. 8, q_e values decreased from 133.3 mg g^{-1} to 25.6 mg g^{-1} as the adsorbent dosage was increased from 10 to 40 mg. It is speculated that this phenomenon was due to the added larger amount of adsorbent and unsaturated active site because the removal efficiency was close to 100% when the

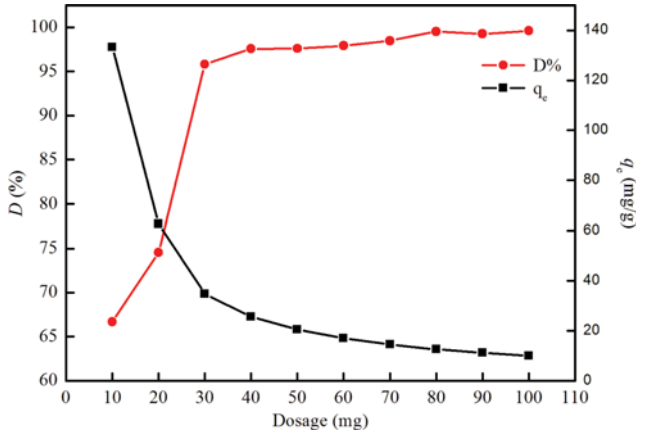

Fig. 8. Effect of adsorbent dose on CR adsorption (conditions: CR concentration, 200 mg L^{-1}; contact time, 120 min; adsorbent dose, 2 g L^{-1}; adsorption temperature: room temperature).

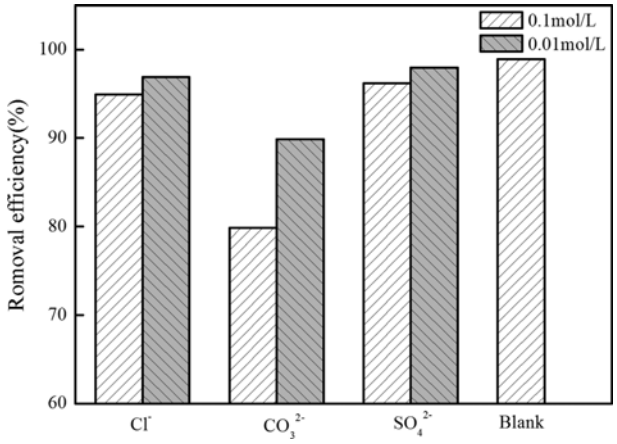

Fig. 9. Effect of interfering ions on CR adsorption (condition: CR concentration, 200 mg L^{-1}; contact time, 120 min; adsorbent dose, 3 g L^{-1}; adsorption temperature: room temperature).

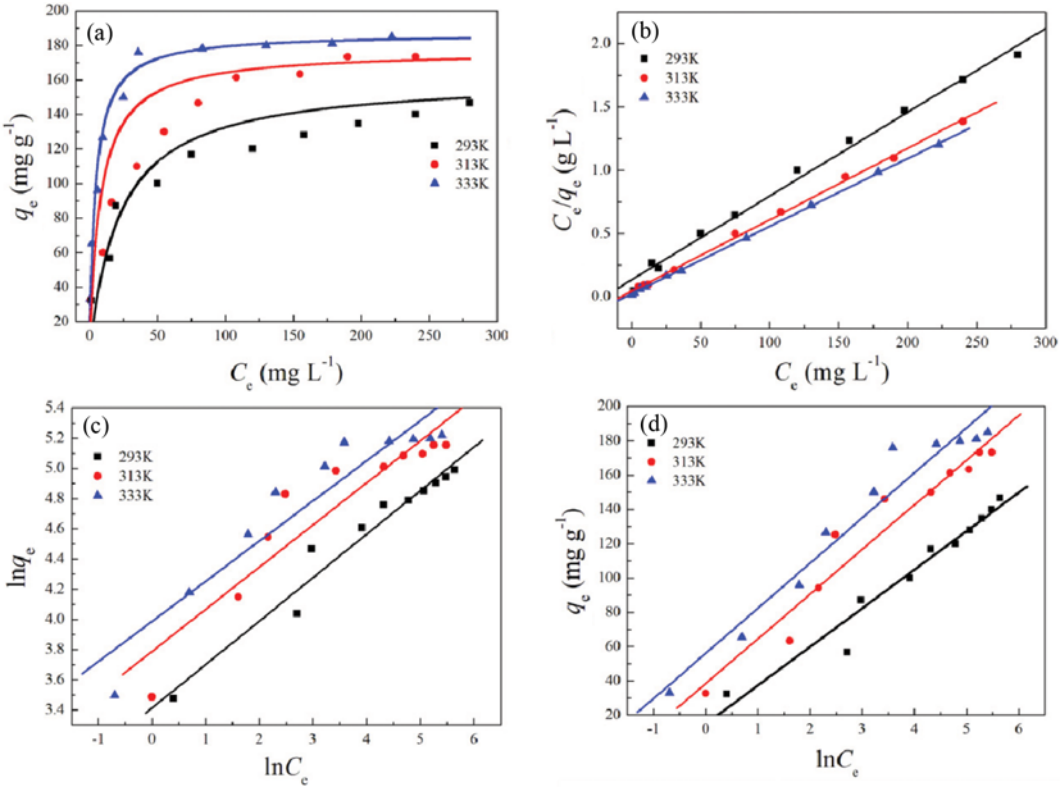

Fig. 10. Adsorption equilibrium isotherms of CR on Ni-Al-2 composites at three different temperature (a) and using Langmuir isotherm (b), Freundlich isotherm (c) and Temkin isotherm (d) model.

amount of dosage was 40 mg [29]. Another explanation was the competition of the CR for the active sites available [30]. Further condensation of adsorbent resulted in a decrease in total adsorbent surfaced area available to CR and an increase in diffusion path length. Thus, the amount of adsorbent dosage should not more than 60 mg for further equilibrium and kinetic studies.

3-3. Effect of Interfering Ions

Industrial dye wastewater is complex and contains a variety of interfering ions, which are likely to affect the adsorption efficiency. Therefore, it is important to have the ability of anti-interference of the adsorbent. In this experiment, two sets of adsorption tests were carried out in the presence of Cl^-, CO_3^{2-} and SO_4^{2-} anions with different ions concentrations (0.1 mol L^{-1} and 0.01 mol L^{-1}) (as shown in Fig. 9). The results showed the obtained composites had a strong anti-interference ability. Overall, in the case of several interfering ions existing, Ni-Al-2 composites still had about 90% adsorption efficiency. Only when the concentration of CO_3^{2-} reached 0.1 mol L^{-1} was the adsorption efficiency reduced to 80%. To our knowledge, CO_3^{2-} ion is a planar structure, which is easy to insert into the nano-layer sheet. Therefore, the above result was probably caused by the high charge density of CO_3^{2-} adsorbing on the surface of the adsorbent, which will occupy a large number of active sites and prevent the interaction of dye molecules and adsorbent.

4. Equilibrium Isotherms

The adsorption isotherms make sense to explore the way of CR molecule interacting with the adsorbent surface. Fig. 10(a) shows adsorption isotherms for CR at 293 K, 313 K and 333 K. The equilibrium isotherms not only express the specific relation between the concentration of adsorbate and the adsorption capacity of adsorbents, but also find the best model for the adsorption of CR [31]. The most widely used isotherm models for solid-liquid adsorption are the Langmuir, Freundlich and Temkin isotherms.

The Langmuir isotherm is applicable to monomolecular layer adsorption. The theory is based on the assumption that there are a finite number of binding sites homogeneously distributed over the adsorbent surface, and once the adsorbate occupies a site, no further adsorption can take place at that site. The equation of the Langmuir isotherm is [32] as follows:

$$q_e = \frac{K_L q_m C_e}{1 + K_L C_e}$$

where C_e is the equilibrium concentration of the adsorbate (mg L^{-1}), q_e is the amount of adsorbate adsorbed per unit mass of adsorbent at equilibrium (mg g^{-1}), q_m is the theoretical maximum monolayer adsorption capacity of the adsorbent (mg g^{-1}), and K_L is the Langmuir isotherm constant related to the adsorption energy (L mg^{-1}). A well-known linear expression for the Langmuir isotherm is [33] as follows:

$$\frac{C_e}{q_e} = \frac{C_e}{q_m} + \frac{1}{K_L q_m}$$

The values of K_L and q_m can be determined from the slope and intercept of the linear plot of C_e/q_e versus C_e, as shown in Fig. 10(b).

The Freundlich model is an empirical equation based on sorption on heterogeneous surfaces or surfaces supporting sites of varied affinities. It is assumed that the stronger binding sites are occupied first and that the binding strength decreases with the increasing degree of site occupation [34]. The isotherm is expressed as follows:

$$q_e = K_F C_e^{1/n}$$

where K_F ((mg g^{-1}) (L $mg^{1/n}$)) and n are Freundlich constants related to sorption capacity and sorption intensity of the adsorbent. 1/n gives an indication of the favorability of adsorption. A well-known logarithmic form of the Freundlich isotherm is expressed as follows [35]:

$$\ln q_e = \ln K_F + \frac{1}{n} \ln C_e$$

The values of K_F and n were calculated from the intercept and slope of the plot of $\ln q_e$ versus $\ln C_e$, as shown in Fig. 10(c). It can be seen from Table 2 that the value of exponent n is more than 1, indicating favorable adsorption conditions.

The Temkin isotherm contains a factor that explicitly takes into account the adsorbent-adsorbate interactions. The heat of adsorption of the molecules in the adsorbent surface layer would decrease linearly with coverage. The Temkin isotherm is expressed in its linear form as [34] follows:

$$q_e = B \ln A + B \ln C_e$$

where A is the equilibrium binding constant corresponding to the maximum binding energy (L mg^{-1}) and B is the Temkin constant related to the heat of adsorption. The constants A and B can be determined by a plot of q_e versus $\ln C_e$, as shown in Fig. 10(d).

Table 2 lists all the correlation coefficients, the R^2 values, and the constants from the three isotherm models. According to the correlation coefficient (R^2), the Langmuir isotherm model gave the highest R^2 values of 0.999, indicating that it was the most suitable equation to describe the adsorption equilibrium of the CR on the samples prepared. Moreover, the q_m was calculated as 186.9 mg g^{-1}, which was quite close to the true value. From Fig. 10(a), the values of q_m of three temperatures were increasing with the temperature. By that reasoning, the endothermic property of the adsorption

Table 2. Isotherm parameters obtained for the adsorption of CR on the NiO/Al_2O_3 composites samples

K	Langmuir isotherm model			Freundlich isotherm model			Temkin isotherm model		
	q_{max}	K_L	R^2	K_F	n	R^2	A	B	R^2
293	161.3	0.0462	0.993	30.66	3.47	0.958	1.94	22.50	0.958
313	177.0	0.128	0.998	44.15	4.58	0.871	4.36	26.09	0.942
333	186.9	0.234	0.999	53.92	4.76	0.891	8.42	26.32	0.950

q_{max} (mg g^{-1}), K_L (L mg^{-1}), K_F (mg/g(L $mg^{-1})^{1/n}$)

Table 3. Comparison of maximum adsorption capacity of various adsorbents for CR removal

Adsorbent	q_m (mg g^{-1})	References
Boehmite hollow core/shell microspheres	111.3	[17]
Hierarchical NiO nanosheets	151.7	[37]
Hierarchical spindle-like γ-Al_2O_3	176.7	[38]
NiO(111) nanosheets	36.1	[39]
Nanorod-like mesoporous γ-Al_2O_3	83.8	[40]
Biomorphic CLDH	119.9	[41]
Hollow hierarchical MnO_2	60	[42]
Mg-Al-layered double hydroxide	37	[43]
NiO-SiO_2 hollow microspheres	204	[44]
Hierarchical porous NiO/Al_2O_3	186.9	This work

process [36], also can be verified from K_L and K_F (the coefficient of Langmuir model and Freundlich model, respectively.) which showed the heat of CR adsorption increased with increasing in temperature. The comparison of the maximum adsorption capacity with other adsorbents is shown in Table 3. Result of the comparison showed that the proposed NiO/Al_2O_3 composite has a relatively high adsorption capacity, demonstrating a potentially efficient adsorbent for pollution control.

5. Adsorption Kinetic Studies

The kinetics of adsorption describes the rate of CR dyes onto the NiO/Al_2O_3 composites and this rate control the equilibrium time [45]. In this work, the kinetics of adsorption were studied at three temperatures and solution concentration and all in the rapid stirring condition, as shown in Fig. 11(a) and Fig. 12(a). It can be seen the two adsorption progresses were initially rapid and then became slow and stagnated with the increase in contact time, and the higher concentration and temperature led to the faster adsorption rate and a greater amount of equilibrium adsorption. It is also observed that adsorption was rather quick, and after 60 min, complete adsorption equilibrium was obtained (see Fig. S4).

To adequately correlate the experiment data, several kinetic models have been used to study the kinetics of the adsorption process: the pseudo-first-order, pseudo-second-order and intra-particle diffusion kinetic models.

A linear form of pseudo-first-order model is described as follows [46]:

$$\ln(q_e - q_t) = \ln q_e - k_1 t$$

where q_e and q_t are the amount of adsorbate adsorbed (mg g^{-1}) at equilibrium and at any instant of time t (min), respectively, and k_1 is the rate constant of pseudo-first-order adsorption (min^{-1}). The constants k_1 can be determined by a plot of $\ln(q_e - q_t)$ versus t, as shown in Fig. 11(b) and Fig. 12(b).

The pseudo-second-order kinetics may be expressed in a linear form as [47,48] follows:

$$\frac{t}{q_e} = \frac{1}{k_2 q_e^2} + \frac{1}{q_e} t$$

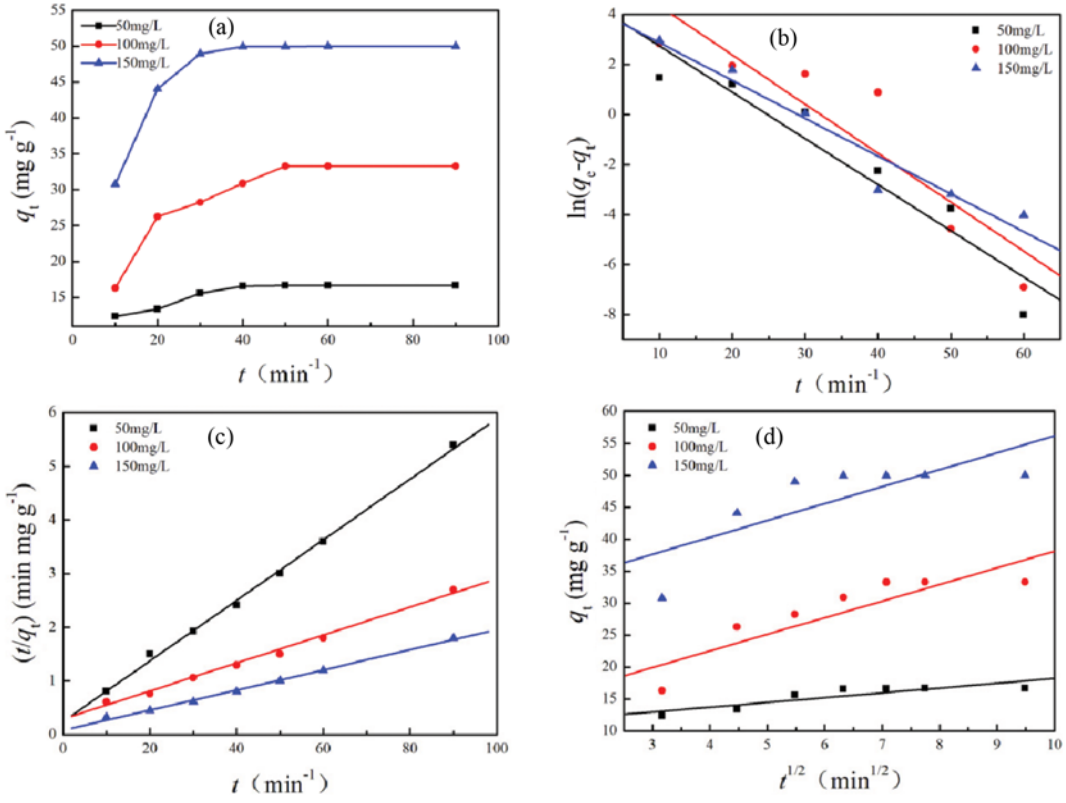

Fig. 11. Adsorption kinetics of CR on Ni-Al-2 composites at three different initial CR concentrations (a) and using pseudo-first-order (b), pseudo-second-order (c) and intra- particle diffusion (d) model.

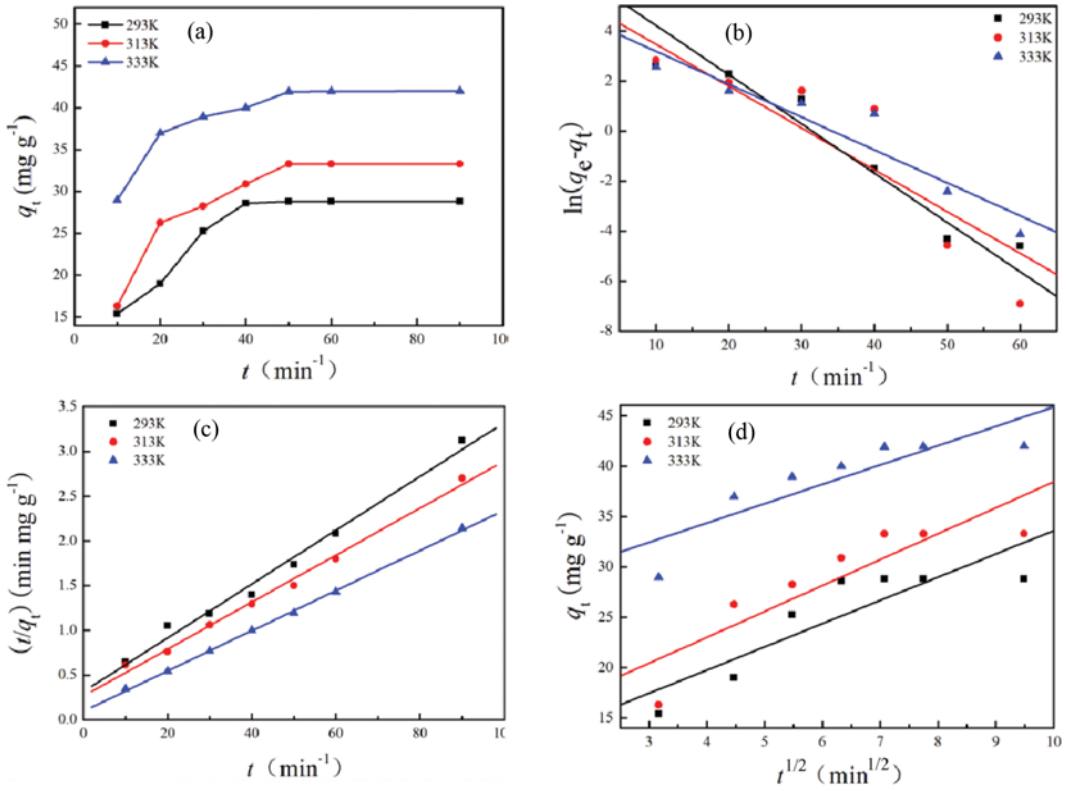

Fig. 12. Adsorption kinetics of CR on Ni-Al-2 composites at three different temperature (a) and using pseudo-first-order (b), pseudo-second-order (c) and intra- particle diffusion (d) model.

Table 4. Kinetic models parameters obtained for the adsorption of CR on the NiO/Al_2O_3 composites

C_0	Pseudo-first-order			Pseudo-second-order			Intra-particle diffusion		
	q_e	K_1	R^2	q_e	K_2	R^2	C	k_p	R^2
50	97.42	−0.185	0.906	17.71	0.013	0.998	10.71	0.7513	0.765
100	538.7	−0.196	0.801	38.23	0.002	0.994	12.16	2.594	0.801
150	79.24	−0.151	0.940	53.36	0.004	0.996	29.70	2.646	0.608

C (mg L^{-1}), q_e (mg g^{-1}), k_1 (min^{-1}), k_2 (g (mg min)$^{-1}$)

Table 5. Kinetic models parameters obtained for the adsorption of CR on the NiO/Al_2O_3 composites

T	Pseudo-first-order			Pseudo-second-order			Intra-particle diffusion		
	q_e	K_1	R^2	q_e	K_2	R^2	C	k_p	R^2
293	171.7	−0.185	0.932	33.22	0.013	0.987	10.54	2.306	0.769
313	492.6	−0.196	0.841	38.04	0.002	0.993	12.73	2.571	0.775
333	90.75	−0.151	0.896	44.48	0.004	0.999	26.69	1.919	0.748

T (K), q_e (mg g^{-1}), k_1 (min^{-1}), k_2 (g (mg min)$^{-1}$)

where k_2 is the equilibrium rate constant of pseudo-second-order adsorption (g (mg·min)$^{-1}$). The constants k_2 can be determined by a plot of t/q_t versus t, as shown in Fig. 11(c) and Fig. 12(c).

Table 4 and Table 5 list the q_e values, the R^2 values and the constants k according the pseudo-first-order model and pseudo-second-order model for adsorption of CR onto the NiO/Al_2O_3 composites samples at three different temperature and CR solution concentration. It was observed that the pseudo-first-order model did not fit well with the result, according to rate constant (k_1) and q_e (see Table 4 and Table 5) along with the correlation coefficients (R^2). It was found that q_e values predicted did not agree with the experimental values. From different temperatures and different concentrations, the same conclusion can be reached. Interestingly, all of the experiment data showed better agreement with the pseudo-second-order kinetic model according to higher correlation coefficients (R^2>0.987), indicating that the adsorption process was dom-

inated by the chemical adsorption. Moreover, the q_e values predicted from the pseudo-second-order model were more in accordance with the experimental q_e values. The result also indicates that the adsorption of CR dye probably proceeded through surface adsorption until the surface vacant sites were fully occupied.

To further study the rate controlling steps affecting the kinetics of adsorption, the intra-particle diffusion kinetic models was borrowed, which model is expressed as [49] follows:

$$q_t = k_p t^{1/2} + C$$

where C is the intercept and k_p is the intraparticle diffusion rate constant (mg g^{-1} min^{-1}), which can be determined from the slope of the linear plot of q_t versus $t^{1/2}$, as shown in Fig. 11(d) and Fig. 12(d). Based on theories developed by Weber and Morris, the intercept of the plot reflects the boundary layer effect. The larger value the intercept has, the greater the contribution of the surface sorption will be made in the rate controlling step [50]. The constant C values and k_p values are listed in Table 4 and Table 5. The constant C was found to increase from 10.71 to 29.70 mg g^{-1} and from 10.54 to 26.69 mg g^{-1} at three different concentrations and different temperatures, respectively. Intraparticle diffusion will be the sole rate-controlling step, if the regression of q_t versus $t^{1/2}$ is linear and passes through the origin. Whereas, it was found that the R^2 values (in Table 4 and Table 5) were quite low and the linear plots (in the Fig. 11(d) and Fig. 12(d)) at each temperature or concentration did not pass through the origin, indicating that the intraparticle diffusion was not the sole rate-controlling step.

6. Reusability of NiO/Al_2O_3 Composites

To further study the stability of the NiO/Al_2O_3 composites, the experiments were investigated by carrying out recycling adsorption five times. The regenerated sample was tested by adsorption of CR and regenerated repeatedly using the previous method, as shown in Scheme 2. Five cycles of regeneration and adsorption process were performed to examine the adsorption stability of the NiO/Al_2O_3 composites, and the results are shown in Fig. 13. Its adsorption performance kept almost unchanged with an increase of cycle times, the adsorption efficiency of the original NiO/Al_2O_3 composites reached 94.6%, and the adsorption efficiency of the

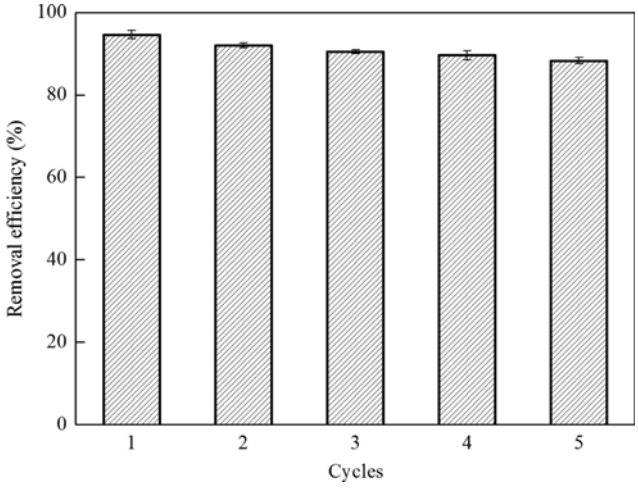

Fig. 13. CR adsorption efficiency on the Ni-Al-2 composites as a function of the cycles (condition: adsorption time, 120 min; adsorption temperature: 313 K).

adsorbents decreased slightly to 88.3% with consecutive adsorption-regeneration process. According to previous reports, the samples could maintain such high adsorption efficiency during the five cycles, mainly due to the good crystallization of samples, which protected the morphology and microstructure from damage [4]. This experiment showed that CR adsorbed on the surface of adsorbents was removed relatively completely, and the regenerated adsorbents also exhibited a good stability of CR adsorption.

7. Tentative Mechanism of Adsorption on NiO/Al_2O_3 Composites

FTIR spectra of NiO/Al_2O_3 before (a), after (b) the CR adsorption and the NiO/Al_2O_3-CR (c) are presented in Fig. 14. The major differences are: the weak absorption band at 3,359 cm^{-1} (Fig. 14(a)), belonging to the stretching vibration of -OH in the NiO/Al_2O_3 composites, shifted to broadened and strengthened wave number 3,461 cm^{-1} after CR adsorption (Fig. 14(b)), corresponding to the stretching vibration of -OH and -NH groups. Meanwhile, the strong peak at 3,466 cm^{-1} could be mainly assigned to the overlap of -OH and

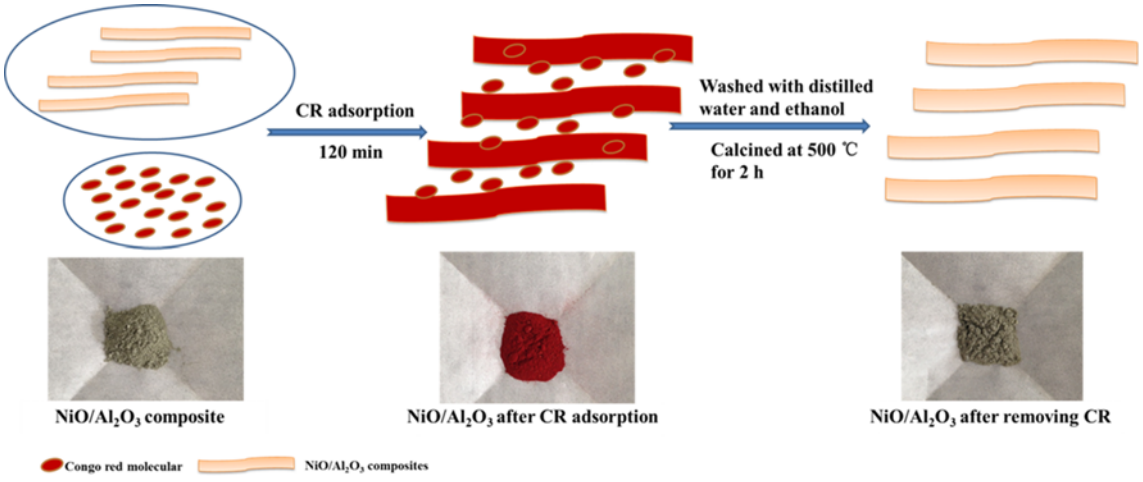

Scheme 2. The reusable process of NiO/Al_2O_3 composites.

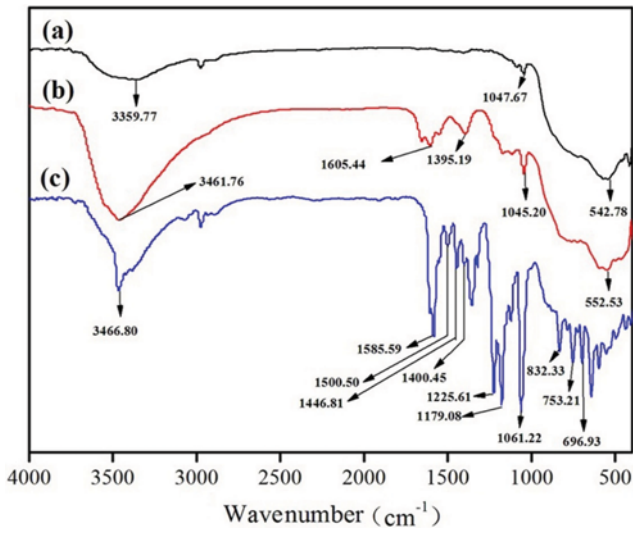

Fig. 14. FTIR of NiO/Al_2O_3 composites before (a), after (b) CR adsorption and (c) NiO/Al_2O_3-CR.

-NH stretching vibrations (Fig. 14(c)). The band at 1,585 cm^{-1}, assigned to -N=N- stretching (Fig. 14(c)), diminished after adsorption (Fig. 14(b)). Also, the strong band at 1,225, 1,179 and 1,062 cm^{-1}, corresponding to the S=O stretching (Fig. 14(c)), disappeared after adsorption (Fig. 14(b)). The above results suggested that the $-NH_2$, -N=N- and $-SO_3$ groups of CR could be involved in the adsorption process. Moreover, the bands at 1,500, 1,446 and 1,400 cm^{-1}, assigned to aromatic skeletal vibrations, were reduced shifted after adsorption. The absorption bands at 832, 753 and 696 cm^{-1}, attributed to typical adsorption of aromatic skeletal groups, were reduced after adsorption. Compared with the IR spectrum of NiO/Al_2O_3 before dye adsorption (Fig. 14(b)), the new absorption bands (1,605, 1,395, 1,045 and 552 cm^{-1}) were shown in NiO/Al_2O_3 after dye adsorption. As a result, CR on NiO/Al_2O_3 was probably conducted by chemisorption or chemical activation, and similar results also were reported in previous studies [51,52]. According to the results of IR analysis, a tentative schematic diagram of CR adsorption on NiO/Al_2O_3 is shown in supplementary information (Fig. S5).

CONCLUSIONS

Hierarchical porous NiO/Al_2O_3 composites were successfully synthesized by a two-step hydrothermal method and combining a subsequent calcination process. The NiO/Al_2O_3 composites combined the advantages of high special surface, micro- and nano-structure and functional adsorption material. High special surface could provide greater contact surface for dyes. Furthermore, the modification of functional material could supply with solid adsorption sites. In addition, micro- and nano-structure have excellent structure stability, which was conducive to the modification and recycling of adsorbents. Ni-Al-2 composites (Ni/Al molar ratio of 1/3) exhibited outstanding adsorption performance. The adsorption efficiency and capacity were found to be over 99.5% and 186.9 mg g^{-1}, respectively. The hierarchical porous NiO/Al_2O_3 composites also presented remarkably higher adsorption efficiency during five recyclings followed by a simple calcination process to removal the adsorbate. Therefore, a desired hierarchical porous NiO/Al_2O_3 with excellent surface features can be applied effectively in wastewater treatment. Finally, this work provides a reproducible, simple, efficient method for the modification of functional material, which will likely exploit more utilization of other materials.

ACKNOWLEDGEMENTS

The National Natural Science Foundation of China (U1507115) and Scientific Research Foundation for Advanced Talents, Jiangsu University (15JDG142) are thanked for their financial support.

SUPPORTING INFORMATION

Additional information as noted in the text. This information is available via the Internet at http://www.springer.com/chemistry/journal/11814.

REFERENCES

1. X. Peng, D. Huang, T. Odoom-Wubah, D. Fu, J. Huang and Q. Qin, *J. Colloid Interface Sci.*, **430**, 272 (2014).
2. S. Yang, L. Wang, X. Zhang, W. Yang and G. Song, *Chem. Eng. J.*, **275**, 315 (2015).
3. G. Crini, *Bioresour. Technol.*, **97**, 1061 (2006).
4. C. Lei, X. Zhu, B. Zhu, J. Yu and W. Ho, *J. Colloid Interface Sci.*, **466**, 238 (2016).
5. R. K. Gautam, V. Rawat, S. Banerjee, M. A. Sanroman, S. Soni, S. K. Singh and M. C. Chattopadhyaya, *J. Mol. Liq.*, **212**, 227 (2015).
6. B. Pal, R. Kaur and I. S. Grover, *J. Ind. Eng. Chem.*, **33**, 178 (2016).
7. L.-N. Jin, X.-Y. Qian, J.-G. Wang, H. Aslan and M. Dong, *J. Colloid Interface Sci.*, **453**, 270 (2015).
8. M. Liu, J. Xu, B. Cheng, W. Ho and J. Yu, *Appl. Surf. Sci.*, **332**, 121 (2015).
9. K. Zare, H. Sadegh, R. Shahryari-ghoshekandi, B. Maazinejad, V. Ali, I. Tyagi, S. Agarwal and V. K. Gupta, *J. Mol. Liq.*, **212**, 266 (2015).
10. V. Gupta, C. Millett, G. K. Walia, S. Kinra, A. Aggarwal, P. Prabhakaran, S. Bhogadi, A. Kumar, R. Gupta and D. Prabhakaran, *J. Public Health*, **23**, 129 (2015).
11. V. K. Gupta and Suhas, *J. Environ. Manage.*, **90**, 2313 (2009).
12. X. Huang, X. Bo, Y. Zhao, B. Gao, Y. Wang, S. Sun, Q. Yue and Q. Li, *Bioresour. Technol.*, **165**, 116 (2014).
13. J. Fang, X. Huang, X. Ouyang and X. Wang, *Chem. Eng. J.*, **270**, 309 (2015).
14. L. Zhang, X. Jiao, D. Chen and M. Jiao, *Eur. J. Inorg. Chem.*, **2011**, 5258 (2011).
15. C. Ottone, V. Farías Rivera, M. Fontana, K. Bejtka, B. Onida and V. Cauda, *J. Mater. Sci. Technol.*, **30**, 1167 (2014).
16. C. Peng, J. Zhang, Z. Xiong, B. Zhao and P. Liu, *Micropor. Mesopor. Mater.*, **215**, 133 (2015).
17. W. Cai, J. Yu, B. Cheng, B.-L. Su and M. Jaroniec, *J. Phys. Chem. C.*, **113**, 14739 (2009).
18. X. Li, J. Feng, J. Guo, A. Wang, R. Prins, X. Duan and Y. Chen, *J. Catal.*, **334**, 116 (2016).
19. T. Wang, L. Chang, B. Hatton, J. Kong, G. Chen, Y. Jia, D. Xiong

and C. Wong, *Mater. Sci. Eng. C.*, **43**, 310 (2014).
20. T. Fan, X. Li, J. Ding, D. Zhang and Q. Guo, *Micropor. Mesopor. Mater.*, **108**, 204 (2008).
21. S. Cho, S. Kim, E. Oh, S.-H. Jung and K.-H. Lee, *CrystEngComm*, **11**, 1650 (2009).
22. P. Lv, H. Zhao, Z. Zeng, C. Gao, X. Liu and T. Zhang, *Appl. Surf. Sci.*, **329**, 301 (2015).
23. R. Wang, Q. Li, D. Xie, H. Xiao and H. Lu, *Appl. Surf. Sci.*, **279**, 129 (2013).
24. X.-H. Zhang, X.-X. Li, H. Chen, T.-B. Li, W. Su and S.-D. Guo, *Mater. Des.*, **92**, 58 (2016).
25. S. B. Chandrasekhar, S. Sudhakara Sarma, M. Ramakrishna, P. Suresh Babu, T. N. Rao and B. P. Kashyap, *Mater. Sci. Eng. A.*, **591**, 46 (2014).
26. M. A. Behnajady and S. Bimeghdar, *Chem. Eng. J.*, **239**, 105 (2014).
27. F. Motahari, M. R. Mozdianfard and M. Salavati-Niasari, *Process. Saf. Eviron.*, **93**, 282 (2015).
28. X. Liu, Y. Yan, Z. Da, W. Shi, C. Ma, P. Lv, Y. Tang, G. Yao, Y. Wu and P. Huo, *Chem. Eng. J.*, **241**, 243 (2014).
29. K. S. Tong, M. J. Kassim and A. Azraa, *Chem. Eng. J.*, **170**, 145 (2011).
30. S. Chen, Q. Yue, B. Gao and X. Xu, *J. Colloid Interface Sci.*, **349**, 256 (2010).
31. T. Zhang, Q. Li, Y. Liu, Y. Duan and W. Zhang, *Chem. Eng. J.*, **168**, 665 (2011).
32. A. Y. Dursun and Ç. S. Kalayci, *J. Hazard. Mater.*, **123**, 151 (2005).
33. Z. P. Liang, Y. Q. Feng, S. X. Meng and Z. Y. Liang, *Process Biochem.*, **40**, 3218 (2005).
34. B. H. Hameed, D. K. Mahmoud and A. L. Ahmad, *J. Hazard. Mater.*, **158**, 65 (2008).
35. L. J. Kennedy, J. J. Vijaya, G. Sekaran and K. Kayalvizhi, *J. Hazard. Mater.*, **149**, 134 (2007).
36. Q.-S. Liu, T. Zheng, P. Wang, J.-P. Jiang and N. Li, *Chem. Eng. J.*, **157**, 348 (2010).
37. B. Cheng, Y. Le, W. Cai and J. Yu, *J. Hazard. Mater.*, **185**, 889 (2011).
38. W. Cai, J. Yu and M. Jaroniec, *J. Mater. Chem.*, **20**, 4587 (2010).
39. Z. Song, L. Chen, J. Hu and R. Richards, *Nanatechnol.*, **20**, 275707 (2009).
40. W. Cai, Y. Hu, J. Chen, G. Zhang and T. Xia, *CrystEngComm*, **14**, 972 (2012).
41. R. Wang, Q. Li, N. Duan, T. Zhang and H. Lu, *Res. Chem. Intermed.*, **41**, 7899 (2015).
42. J. Fei, Y. Cui, X. Yan, W. Qi, Y. Yang, K. Wang, Q. He and J. Li, *Adv. Mater.*, **20**, 452 (2008).
43. R.-r. Shan, L.-g. Yan, Y.-m. Yang, K. Yang, S.-j. Yu, H.-q. Yu, B.-c. Zhu and B. Du, *J. Ind. Eng. Chem.*, **21**, 561 (2015).
44. C. Lei, X. Zhu, B. Zhu, J. Yu and W. Ho, *J. Colloid Interface Sci.*, **466**, 238 (2016).
45. K. Singh and S. Mohan, *Appl. Surf. Sci.*, **221**, 308 (2004).
46. R. Leyva-Ramos, J. Rivera-Utrilla, N. A. Medellin-Castillo and M. Sanchez-Polo, *Chem. Eng. J.*, **158**, 458 (2010).
47. Y.-S. Ho, *Water Res.*, **40**, 119 (2006).
48. Y. S. Ho and G. McKay, *Water Res.*, **34**, 735 (2000).
49. H. Zaghouane-Boudiaf and M. Boutahala, *Int. J. Miner. Process.*, **100**, 72 (2011).
50. H. Zaghouane-Boudiaf, M. Boutahala, C. Tiar, L. Arab and F. Garin, *Chem. Eng. J.*, **173**, 36 (2011).
51. L. Wang and A. Wang, *J. Hazard. Mater.*, **160**, 173 (2008).
52. R. Ahmad and R. Kumar, *Appl. Surf. Sci.*, **257**, 1628 (2010).

Supporting Information

Structural evolution of hierarchical porous NiO/Al_2O_3 composites and their application for removal of dyes by adsorption

Jian Rong*, Tao Zhang*,, Fengxian Qiu*,†, and Mingliang Chen***

*School of Chemistry and Chemical Engineering, Jiangsu University, Zhenjiang 212013, Jiangsu Province, China
**Institute of Green Chemistry and Chemical Technology, Jiangsu University, Zhenjiang 212013, Jiangsu Province, China
(*Received 23 April 2016 • accepted 1 August 2016*)

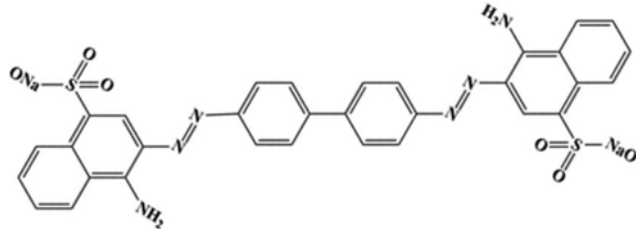

Fig. S1. The molecular structure of Congo red.

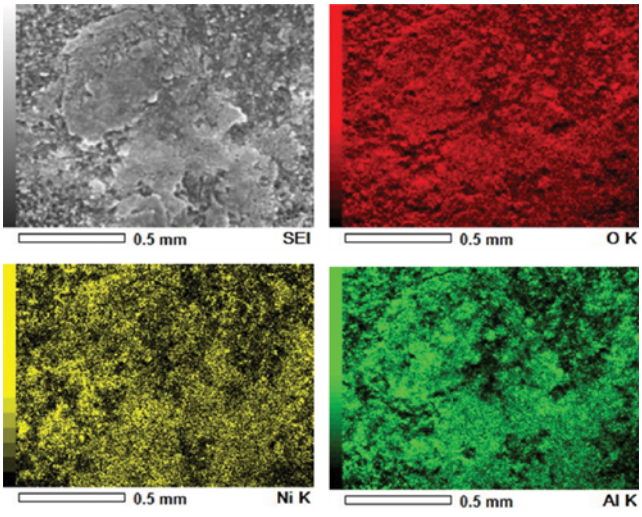

Fig. S2. The EDS elemental mapping of Ni-Al-2.

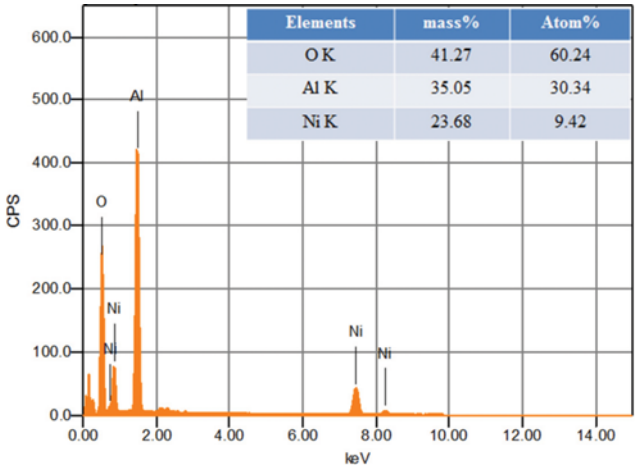

Fig. S3. The EDS result of Ni-Al-2 samples.

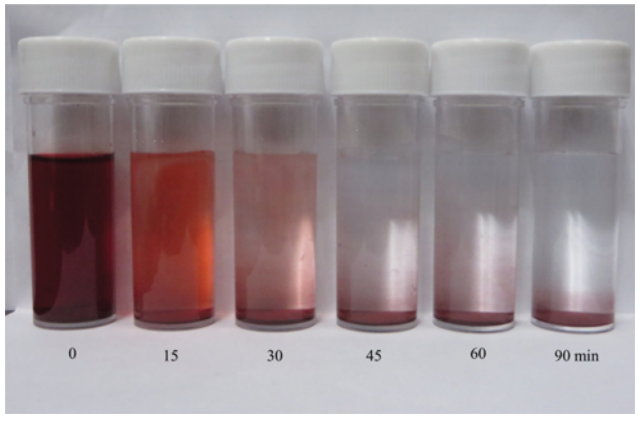

Fig. S4. The picture of adsorption effects in the presence of the Ni-Al-2 after time intervals of 0, 15, 30, 45, 60, and 90 min.

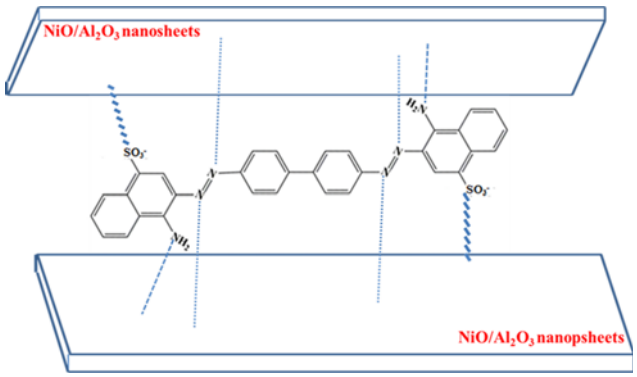

Fig. S5. Tentative schematic diagram of CR adsorption on NiO/Al_2O_3.